Discretization of Macroscopic Transport Equations on Non-Cartesian Coordinate Systems

Michael Spevak and Tibor Grasser, *Senior Member, IEEE*

***Abstract*—We discuss discretization schemes for the Poisson equation, the isothermal drift-diffusion equations, and higher order moment equations derived from the Boltzmann transport equation for general coordinate systems. We briefly summarize the method of dimension reduction when the problem does not depend on one coordinate. Discretization schemes for dimension-reduced coordinate systems are introduced, which provide curvilinear coordinate systems. In addition to the reduction of the dimensionality, another benefit of these curved coordinate systems is that the domain approximation is more accurate, and therefore, the mesh point density can be kept smaller compared to the original problem. We obtain a discretization scheme for the isothermal drift-diffusion equation in closed from. For higher order transport equations, we use the approximation method of optimum artificial diffusivity and generalize it for non-Cartesian coordinate systems. For the special case of cylindrical coordinates, we can show that it is not necessary to introduce special discretization schemes apart from the standard Scharfetter–Gummel scheme.**

***Index Terms*—Coordinate systems, device simulation, discretization, higher order transport models, rotational symmetry, TCAD, transport models.**

I. Introduction

In order to solve the Poisson equation and the drift-diffusion equations, finite differences or the method of finite volumes [1] are commonly applied. Due to a particular device design, for instance of short-channel large-width MOS transistors, it is often justified to assume that the electrical behavior is independent of the third coordinate. Thus, the problem can be reduced to two dimensions in a straightforward way. The same principle can be applied to other separable orthogonal coordinate systems. However, to the best of our knowledge, only rotationally symmetric cylindrical coordinate systems have been used so far in the context of semiconductor-device simulation. If the material parameters and boundary conditions are independent from a coordinate, it is possible to simplify the problem by elimination.

For the special case of cylindrical structures, rotational symmetry can be exploited (see Fig. 1). In this case, the problem can easily be described in polar cylindrical coordinates, because the geometry is completely independent of the azimuthal angle φ. Several attempts have been made to reduce the calculation effort of a 3-D problem to two dimensions by taking advantage of this cylindrical symmetry. For instance, the simulator BAMBI [2] approximates the Poisson equation as well as the continuity equations for rotational symmetric structures using standard finite boxes. This approach is based on using discretized cylindrical differential operators in the equation systems but relies on orthogonal grids and is limited to Manhattan-like geometries, and grid refinement inevitably leads to an unnecessary large number of grid points.

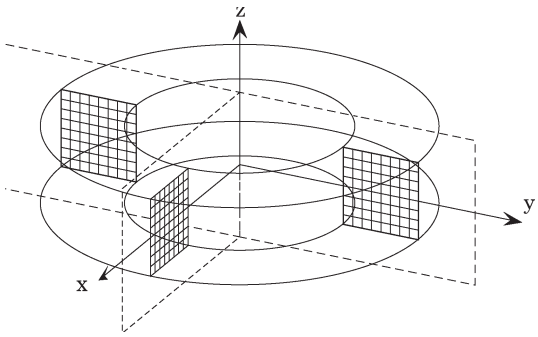

Fig. 1. Rotational symmetry.

The simulation tool TRINE [3] introduces geometry adaptation for the method of finite volumes. This approach is limited to orthogonal grids and results in algebraically different formulas than the Scharfetter–Gummel scheme. A different discretization scheme is obtained, because the drift-diffusion equation is solved assuming a linear potential distribution instead of the consistent logarithmic distribution, which is obtained from the Poisson equation. As a consequence, the discretization scheme contains elliptic integrals.

Commercial simulators like Dessis [4] and Medici [5] offer simulation in a cylindrical coordinate system, without going into details on the implementation.

The various issues regarding discretization schemes for general coordinate systems will be thoroughly investigated in the following. In addition, the discretization of higher order moment equations [6], [7] is discussed.

II. Equation Types

In the following section, the mathematical problem is specified. The equations we have to solve are the Poisson equation as well as the transport equations for electrons and holes, which can be written in terms of general self-adjoint operators and, therefore, can be transformed into integral form by applying the Gauß integral theorem so as to discretize the equations by finite volumes.

Manuscript received June 27, 2005; revised October 12, 2005. The work of M. Spevak was supported by the "Christian Doppler Forschungsgesellschaft," Vienna, Austria. This paper was recommended by Associate Editor W. Schoenmaker.

The authors are with the Institute for Microelectronics, TU Vienna, 1040 Vienna, Austria.

Digital Object Identifier 10.1109/TCAD.2007.891378

0278-0070/$25.00 © 2007 IEEE

A. Problem Formulation

The Poisson equation describes the relation between the charge and the electrostatic potential and reads for inhomogeneous and anisotropic media

$$\mathbf{D} = \underset{\sim}{\varepsilon}\mathrm{grad}\psi \tag{1}$$

$$\mathrm{div}(\mathbf{D}) = \varrho. \tag{2}$$

Here, $\underset{\sim}{\varepsilon}$ is a material parameter, and ϱ denotes the charge density. The flux term of a fairly general drift (convection)-diffusion equation can be written as [7]

$$\mathbf{J}^{(k)} = A^{(k)}\left(\mathrm{grad}\left(\xi^{(k)}T^{(k)}\right) - L^{(k)}\xi^{(k)}\mathrm{grad}\psi\right) \tag{3}$$

while the associated stationary-balance equation reads [7]

$$\mathrm{div}\mathbf{J}^{(k)} = \mathrm{grad}\psi\cdot\mathbf{J}^{(k-1)} + \xi\frac{T^{(k)} - T_{\mathrm{eq}}^{(k)}}{\tau^{(k)}}. \tag{4}$$

Equations (3) and (4) cover the drift-diffusion current relations [1], energy-transport models [6], [8], [9], and higher order moment models [7] as special cases. For the isothermal drift-diffusion equations, ξ is the carrier concentration n, and the temperature is assumed equal to the lattice temperature being constant all over the simulation domain. For the electron current and the energy-flux relation of the energy-transport model, one obtains $\xi^{(0)} = n$, $T^{(0)} = T_n$, $\xi^{(1)} = nT_n$, and $T^{(1)} = T_n$.

B. Metrics and Separation

In the following, it is clarified under which circumstances an equation system is separable for a certain kind of equation. This means that the equation can be solved with a separation ansatz. We use a weaker formulation, because we only separate one coordinate. Each coordinate system can be described by a continuous transformation as well as a back transformation to a reference system. In general, the new coordinates x_i are obtained from the Cartesian coordinates c_i via the nonlinear coordinate transformation

$$x_i = \Theta_i(c_1, c_2, c_3). \tag{5}$$

Each coordinate system can be represented locally by the position vector $\mathbf{r}$. The metric tensor $\underset{\sim}{g}$ of the coordinate system can be obtained from

$$g_{ij}^2 = \partial_{x_i}\mathbf{r}\cdot\partial_{x_j}\mathbf{r}. \tag{6}$$

If only the diagonal elements g_{ii} are nonzero, $\underset{\sim}{g}$ is a diagonal tensor and the coordinate system is locally orthogonal or orthogonal. In the following, we will restrict our discussion to orthogonal coordinate systems and denote the diagonal elements of the metric tensor as $g_i = g_{ii}$ (see Table I for some examples). For such a coordinate system, the divergence operator is expressed as

$$\mathrm{div}(\mathbf{F}) = \frac{1}{g_1g_2g_3}\Big(\partial_{x_1}(g_2g_3F_1) + \partial_{x_2}(g_1g_3F_2) + \partial_{x_3}(g_1g_2F_3)\Big) \tag{7}$$

TABLE I
TABLE OF THE METRIC COEFFICIENTS OF COMMON COORDINATE SYSTEMS. NOTE THAT THE h PARAMETERS ARE INTRODUCED IN (21)

Coordinate	h_1	h_2	h_3
Cartesian	1	1	1
Cylindrical r	r	r	r^{-1}
Spherical	$r^2\sin\theta$	$\sin\theta$	$1/\sin\theta$

while the gradient operator reads

$$\mathrm{grad}(f) = \sum_{i=1}^{d}\frac{1}{g_i}\partial_{x_i}f\mathbf{e}_i. \tag{8}$$

Physical and mathematical problems can be simplified using separation methods, if all geometrical and physical quantities are independent from the value of a coordinate. In general, the separation ansatz implies that the solution is of the form

$$\xi(x_1, x_2, x_3) = \xi_S(x_1, x_2)\zeta(x_3). \tag{9}$$

A necessary criterion for the separability of a coordinate is that the metric coefficients g_1 and g_2 do not depend on x_3. Otherwise, the self-adjoint equation would contain x_3, which is a contradiction to basic assumptions of separability. One coordinate system, which fulfills this criterion, is the cylindrical system.

III. DISCRETIZATION

In the following section, we present discretization schemes for (2) and (4). As the main part of this paper, the discretization of the flux relations (1) and (3) will be given in the next section. The given simulation domain is separated into a finite number of subdomains, so-called box volumes by the Voronoi tessellation [10]. The differential equations are written in integral form, and the Gauß integral theorem can be applied to the divergence integrals. The volume integration can be transformed into a boundary integration, which is approximated by a piecewise multiplication of fluxes and boundary areas. The discretization of the fluxes is treated in Section IV.

After the discretization, we obtain a set of coupled nonlinear ordinary differential equations. Usually, they are solved with the Newton method. We briefly outline the linearization procedure, and as a final result, we obtain the Jacobian matrix of the nonlinear problem.

A. Calculation of Surfaces and Volumes

First, the box volumes and surfaces are calculated in arbitrary coordinates. Both can be derived by integration in a straightforward manner. As mentioned, the separation ansatz is only possible if the geometry of the simulation domain is invariant with the coordinate x_3. The geometric structure remaining after separation of the third coordinate is called Γ. The partition of the simulation domain in box volumes is performed

on Γ. The box volumes can be calculated by the following integration:

$$V = \left(x_3^+ - x_3^-\right) \int_{\mathcal{A}} g_1 g_2 g_3 dx_1 dx_2 \tag{10}$$

$$S = \left(x_3^+ - x_3^-\right) \int_{\partial\mathcal{A}} g_1 g_2 g_3 ds \tag{11}$$

where $\mathcal{A}$ is the projection of the box volume to the cross section Γ. The separated coordinate x_3 is bounded by the interval $[x_3^-, x_3^+]$. For cylindrical coordinate systems with separated x_3 component, (10) and (11) give the well-known Guldin rules

$$S = 2\pi r_{\mathrm{m}} S_\Gamma \quad \text{and} \quad V = 2\pi r_{\mathrm{s}} V_\Gamma \tag{12}$$

where r_{m} denotes the line baricenter and r_{s} the volume baricenter of the rotated volume. The volumes V_Γ and S_Γ denote the volumes and surface elements, respectively, on the structure Γ after dimension reduction.

B. Continuity Equations

For the discretization of the flux equation (3), we use a generalized Scharfetter–Gummel discretization. The original 1-D solution procedure is adapted for 2-D meshes, and a new discretization scheme is derived.

The general discretized flux-conservation equation for the ith box volume is thus obtained as

$$F_{\psi_i} = \sum_{j=1}^{n} D_{ij} \frac{A_{ij}}{d_{ij}} - qV_i(n_i - p_i + N_{A_i} - N_{D_i}) = 0. \tag{13}$$

Analogously, the balance equations associated with the higher order moment fluxes are treated in their integral forms. The flux (3) is rewritten by the use of the Gauß integral theorem

$$\oint_{\partial\mathcal{V}} \mathbf{J}^{(k)} d\mathbf{s} = \int_{\mathcal{V}} \mathrm{grad}\psi \cdot \mathbf{J}^{(k-1)} dV + \int_{\mathcal{V}} \xi^{(k)} \frac{T^{(k)} - T_{\mathrm{eq}}^{(k)}}{\tau^{(k)}} dV. \tag{14}$$

The discretization of the integral of the force term $(\mathrm{grad}\psi \cdot \mathbf{J}^{(k-1)})$ is discussed in [7]. Using (10) and (11), we calculate the surfaces and box volumes, which are inserted into the discretized balance equations. As a final discretization, we thus obtain

$$\begin{aligned} F_{\xi_i}^{(k)} = &- \sum_{j=1}^{N} A_{ij} J_{ij}^{(k)} + \sum_{j=1}^{N} (\psi_j - \psi_i) A_{ij} J_{ij}^{(k-1)} \\ &- V_i \xi_i^{(k)} \frac{T_i^{(k)} - T_{i,\mathrm{eq}}^{(k)}}{\tau_i^{(k)}} \\ = &\, 0. \end{aligned} \tag{15}$$

IV. Flux-Density-Interpolation Schemes

In the following section, the electrical displacement flux $\mathbf{D}$ relation as well as the higher order flux relations are considered.

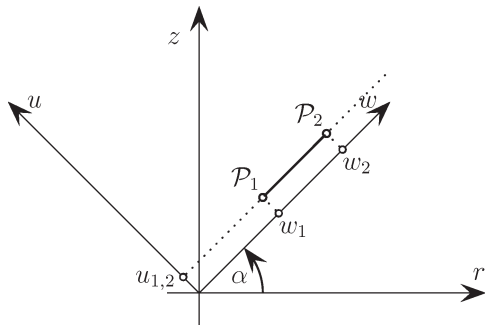

Fig. 2. Rotated coordinate system (w, u) with rotation angle α.

In order to keep the ansatz as consistent as possible, the solution of the local Poisson equation is used to derive the electric field in the macroscopic-transport equations. Consistent with the standard Scharfetter–Gummel method, we assume the projected flux to be constant on an edge. For any flux-conservation equation, the flux density F varies with the component of the metric tensor of the separated variable. For instance, for rotationally cylindrical coordinates, where $g_{\alpha\alpha} = r$ holds, we obtain $rF = \mathrm{const}$.

A. Flux Projection

After the separation of the invariant coordinate x_3, we have reduced the original 3-D problem to two dimensions. Now, the edges, which connect two neighboring points, have to be considered. Note that edges are affine under the back transformation Θ, for instance an isocoordinate line for orthogonal grids. In general, however, these edges are not isocoordinate lines. To facilitate the solution of the differential equations on these edges, a rotated coordinate system is introduced which guarantees that each edge can be described by a longitudinal and a normal component w and u (see Fig. 2)

$$x_1 = w\cos(\alpha) - u\sin(\alpha) \tag{16}$$

$$x_2 = w\sin(\alpha) + u\cos(\alpha). \tag{17}$$

The coordinate variable is normalized to length so as to obtain dimensionless metric coefficients. An edge between the two points then can always be described by a common u coordinate and two boundary coordinates w_1 and w_2. As the flux vector is projected on the edge, the derivative ∂_u vanishes for isotropic media. The gradient can be written in terms of the longitudinal derivative as

$$\partial_{x_i} f = \partial_w f \partial_{x_i} w. \tag{18}$$

Together with the unity vector $\mathbf{e}_w$, we obtain [11]

$$\mathrm{grad} f = \mathbf{e}_w \partial f_w \left(\frac{\cos^2(\alpha)}{g_1} + \frac{\sin^2(\alpha)}{g_2} \right). \tag{19}$$

The Laplace operator results in [11]

$$\begin{aligned} \mathrm{div}(\mathrm{grad} f) = \frac{1}{h_1 h_2 h_3} \big(&\cos^2(\alpha) \partial_w (h_1 \partial_w f) \\ &+ \sin^2(\alpha) \partial_w (h_2 \partial_w f) \big) \end{aligned} \tag{20}$$

with the auxiliary quantities

$$h_n = \frac{\Pi_{j=1}^{3} g_j}{g_n^2}. \tag{21}$$

B. Poisson Equation

The local flux of the Poisson equation is the dielectric displacement, which is proportional to the gradient of the potential. It has to be derived from the center point values of the electrostatic potential ψ. We interpolate the electrostatic potential on a mesh edge, which allows us to calculate the displacement.

In the finite-volume method, the source terms are moved to the center points. Therefore, the interpolation scheme is derived from the homogeneous equation $\mathrm{div}(\underset{\sim}{\varepsilon} \cdot \mathrm{grad}\psi) = 0$, from which follows that charge is concentrated in the center points. In the case of an isotropic medium $\underset{\sim}{\varepsilon} = \mathrm{const}$, the equation simplifies to $\mathrm{div}(\mathrm{grad}\psi) = 0$. The electric field, which is calculated between the two neighboring volume centers, is obtained from the projection of the field strength onto the normalized edge-direction vector $\mathbf{n}$. Thus, we obtain

$$\frac{1}{h_1 h_2 h_3} \left(\partial_{x_1}(h_1 \partial_{x_1}\psi) + \partial_{x_2}(h_2 \partial_{x_2}\psi) \right) = 0. \tag{22}$$

Even though the Poisson equation is assumed to be isotropic in the following sections, the extension to anisotropic media is straightforward. However, the solution of the total equation system can only be rotationally symmetric if the material tensors fulfill the following conditions: All tensor components with the separated coordinate except the diagonal element g_3 have to vanish and, in addition, the tensor components must not depend on the separated coordinate x_3. The matrix representation of a tensor meeting these requirements is

$$\underset{\sim}{g} = \begin{pmatrix} g_1 & g_{12} & 0 \\ g_{12} & g_2 & 0 \\ 0 & 0 & g_3 \end{pmatrix}. \tag{23}$$

Assuming a diagonal tensor in the coordinate directions, these assumptions are met while the anisotropic behavior between the coordinates x_1 and x_2 is neglected. Then, the material parameters and the metric coefficients can be written as one combined tensor. For the following considerations, however, we continue with the isotropic case.

By inserting the rotated coordinate projection, the Poisson equation simplifies to

$$\partial_w \psi \frac{\partial_w H}{H} + \partial_{ww}\psi = 0 \tag{24}$$

with

$$H(w) = \left(\cos^2(\alpha) h_1 + \sin^2(\alpha) h_2 \right)^{-1}. \tag{25}$$

By introducing the boundary conditions at the end points of the edge, we obtain

$$\psi = \psi_i + \Delta\psi \frac{\int_{w_i}^{w} H dw'}{\int_{w_i}^{w_j} H dw'} \tag{26}$$

$$\mathrm{grad}\psi = G \Delta\psi \frac{H}{\int_{w_i}^{w_j} H dw'} \tag{27}$$

where

$$G(w) = \frac{\cos^2(\alpha)}{g_1} + \frac{\sin^2(\alpha)}{g_2}. \tag{28}$$

In Cartesian coordinates, $H = G = 1$, and we obtain the standard linear interpolation of the potential, which corresponds to the conventionally used finite-difference approximation. With the coefficients for cylindrical coordinates (see Table I), the discretization for arbitrary mesh lines in the (r, z) plane results in

$$\mathrm{grad}\psi\Big|_{\overline{r_\mathrm{a}}} = \frac{\Delta\psi}{\Delta w} \frac{r_j - r_i}{\ln(r_j/r_i)} \frac{2}{r_j + r_i} = \frac{\Delta\psi}{\Delta w} \frac{\overline{r_\mathrm{l}}}{\overline{r_\mathrm{a}}}. \tag{29}$$

Here, $\overline{r_\mathrm{a}}$ and $\overline{r_\mathrm{l}}$ denote the arithmetic and the logarithmic mean, respectively, which are generally defined as

$$\overline{x_\mathrm{a}} = \frac{x_i + x_j}{2}$$
$$\overline{x_\mathrm{l}} = \frac{x_i - x_j}{\ln(x_i/x_j)}. \tag{30}$$

This is equivalent with the result obtained by Matsumoto *et al.* [3]. To quantify the deviation from the Cartesian case, we define a geometry $\mathcal{G}$ as the ratio between the general coordinate and Cartesian coordinate discretization of the flux, which is proportional to the gradient operator for the Poisson equation (see Fig. 3). For cylindrical coordinates, we obtain

$$\mathcal{G}_\mathrm{P}^\mathrm{cyl} = \mathrm{grad}\psi \frac{\Delta w}{\Delta\psi} = \frac{\overline{r_\mathrm{l}}}{\overline{r_\mathrm{a}}}. \tag{31}$$

Such a factor will also be introduced for the transport equations and describes the influence of the geometry-corrected interpolation (26).

C. Isothermal Drift-Diffusion Equations

We now turn to the discretization of the transport equations. The isothermal drift-diffusion equations are considered first, because the solution of the resulting ordinary differential equation can be written in an explicit form using integrals. Due to the assumption of $T = \mathrm{const}$, the temperature gradients vanish, and we obtain

$$\mathbf{J} = A \left(T \,\mathrm{grad}(n) - Ln \,\mathrm{grad}(\psi) \right). \tag{32}$$

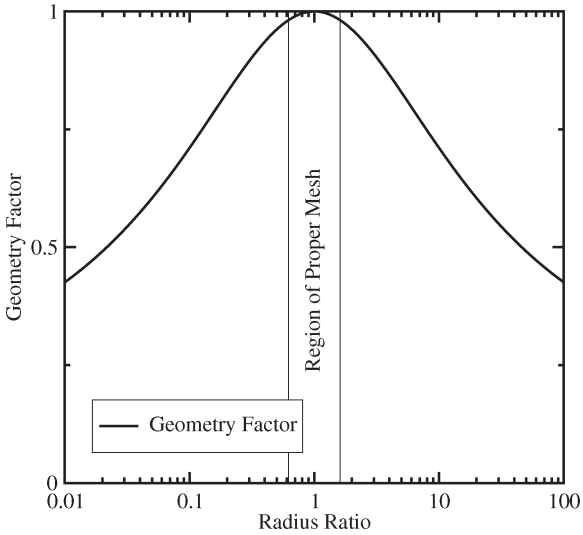

Fig. 3. Geometry factor $\mathcal{G}_{\mathrm{P}}^{\mathrm{cyl}}$ as a function of r_i/r_j on a semilog scale. The region of a properly designed mesh is also shown. The bounds of the radius ratio for a proper mesh definition is determined by the section area.

Projection onto the normalized edge-direction vector $\mathbf{e}_w$ gives

$$\frac{J_w}{ATG(w)} = \partial_w n - n\frac{L\partial_w \psi}{T}. \tag{33}$$

As in the conventional Scharfetter–Gummel scheme, we assume $J_w/(AT)$ to be constant. With the Dirichlet boundary conditions n_i and n_j in the center points, we obtain the projected flux density which can be rewritten in terms of the Bernoulli function so as to obtain a Scharfetter–Gummel-like form

$$J_w = \frac{1}{\Lambda}\left(Mn_j\mathcal{B}(\Lambda) - n_i\mathcal{B}(-\Lambda)\right) \tag{34}$$

with the auxiliary quantities

$$M = \exp\left(K(w_{\mathrm{mid}}) - \Lambda(w_{\mathrm{mid}})\right) \tag{35}$$

$$K(w) = \int_{w_i}^{w} \frac{L\partial_w\psi}{T}dw' = \frac{L}{T}\left(\psi(w) - \psi_i\right) \tag{36}$$

$$\Lambda = -\ln\left(\frac{\exp\left(\frac{L\Delta\psi}{T}\right)}{AT}\int_{w_i}^{w_j}\frac{1}{G(w')} \times \exp\left(K(w')\right)dw' + 1\right). \tag{37}$$

In contrast to the standard Cartesian Scharfetter–Gummel schemes, an additional term appears in front of n_j. Generally, the integrals cannot be evaluated analytically and, therefore, closed-form solutions of (34) do not exist for every coordinate system. However, for some important coordinate systems, analytic solutions exist.

For Cartesian coordinates, we obtain the familiar result

$$J_w^{\mathrm{cart}} = \frac{AT}{\Delta w}\left(n_i\mathcal{B}(\Lambda) - n_j\mathcal{B}(-\Lambda)\right)$$
$$\Lambda = \frac{L\Delta\psi}{T} \tag{38}$$

while, for rotational cylindrical coordinates, we have

$$J_w^{\mathrm{cyl}} = \frac{AT}{\Delta w}\frac{\overline{r_{\mathrm{l}}}}{\overline{r_{\mathrm{a}}}}\left(n_i\mathcal{B}(\Lambda) - n_j\mathcal{B}(-\Lambda)\right)$$
$$J_w^{\mathrm{cyl}} = \frac{\overline{r_{\mathrm{l}}}}{\overline{r_{\mathrm{a}}}}J_w^{\mathrm{cart}}. \tag{39}$$

Note that the method proposed by Matsumoto *et al.* [3] is based on a linear potential interpolation between the box volumes. This ostensibly simpler interpolation leads to elliptic integrals for cylindrical coordinates and cannot be described in terms of analytical functions nor can it be written in a form similar to a Scharfetter–Gummel scheme. It is indeed remarkable that the geometry factor, which appears for the Poisson equation on cylindrical coordinates, is the same as the geometry factor of the isothermal drift-diffusion model

$$\mathcal{G}_{\mathrm{DD}}^{\mathrm{cyl}} = \frac{\overline{r_{\mathrm{l}}}}{\overline{r_{\mathrm{a}}}}. \tag{40}$$

D. Higher Order Moment Equations

The projection of the higher order moment equations or the nonisothermal drift-diffusion equations on rotated coordinates yields equations of the form

$$\frac{J_w}{AGT} = \xi\frac{\left(\partial_w T - L\partial_w\psi\right)}{T} + \partial_w\xi. \tag{41}$$

Not even for Cartesian coordinates can a closed solution of (41) be given [12]. Conventionally, the temperature is assumed to vary linearly between the mesh points [12], [13]. For the generalization to non-Cartesian coordinates, we note that similarly to the Poisson equation, the temperature flux between the mesh points is free of divergence, $\mathrm{div}(\mathrm{grad}\ T) = 0$. Because of the fact that the homogeneous stationary equations for the temperature and the potential are of the same form, we obtain the same interpolation for T as

$$T = T_i + \Delta T\frac{\int_{w_i}^{w} H(w')dw'}{\int_{w_i}^{w_j} H(w')dw'}. \tag{42}$$

To solve the inhomogeneous first-order differential equation (41), the optimum-artificial-diffusivity method [13] is generalized to orthogonal coordinate systems. For the flux equation, the mean coefficient parameters have to be determined from (41) and (42). Following the notation of [13], we write (41) as

$$a^{-1}J_w = \xi b + \partial_w\xi$$
$$a^{-1} = (AGT)^{-1}$$
$$b = \frac{\partial_w T - L\partial_w\psi}{T}. \tag{43}$$

Since we only require the solution of a general first-order ordinary differential equation, the method proposed in [13] can be used to obtain

$$J_w = \frac{\left(\mathcal{B}\left(\langle b\rangle \Delta w\right)\xi_i - \mathcal{B}\left(-\langle b\rangle \Delta w\right)\xi_j\right)}{\langle a^{-1}\rangle \Delta w}$$

$$\langle b\rangle = \int_{w_i}^{w_j} \frac{\partial_w T - L\partial_w \psi}{T} dw' \Delta w^{-1} \tag{44}$$

$$\langle a^{-1}\rangle = \frac{1}{A}\int_{w_i}^{w_j} \frac{1}{GT} dw' \Delta w^{-1}. \tag{45}$$

The mean term $\langle b\rangle$ can be evaluated exactly and is independent of the coordinate system

$$\Lambda = \langle b\rangle = \overline{T_l}^{-1}(\Delta T - L\Delta\psi). \tag{46}$$

The mean term $\langle a^{-1}\rangle$ has to be derived with respect to the coordinate system in use. For Cartesian coordinate systems, we obtain

$$\langle a^{-1}\rangle \Delta w = \frac{1}{A}\int_{w_i}^{w_j} \left(T_i + \frac{\Delta T}{\Delta w}(w - w_i)\right)^{-1} dw' \tag{47}$$

and, therefore

$$J_w = \frac{\overline{T_l} A}{\Delta w}\left(\xi_j \mathcal{B}(\Lambda) - \xi_i \mathcal{B}(-\Lambda)\right) \tag{48}$$

which is of course equivalent to the result obtained by the method of optimum artificial diffusivity [13]. For other coordinate systems, the integrals cannot be evaluated explicitely. By the use of the mean-value theorem of integral calculus, we can split the integrand in two terms: one geometry-dependent term and a temperature-dependent term. The temperature-dependent term will be expressed by some kind of mean value and is denoted as $\overline{T} = T(\overline{w})$. With that assumption, we obtain

$$\int_{w_i}^{w_j} \frac{1}{GT} dw' = \overline{T}^{-1} \int_{w_i}^{w_j} \frac{1}{G} dw'. \tag{49}$$

As the metric tensor coefficients g_1 and g_2 are equal to unity for Cartesian and cylindrical coordinates, the integral (49) can be integrated easily. For other coordinate systems, the geometry correction in $\langle a^{-1}\rangle$ can be determined by numerical integration.

For cylindrical coordinate systems, we have

$$\langle a^{-1}\rangle \Delta w = \frac{\Delta w}{A\overline{T}} \tag{50}$$

and, finally

$$J_w = \frac{\overline{T} A}{\Delta w}\left(\xi_j \mathcal{B}(\Lambda) - \xi_i \mathcal{B}(-\Lambda)\right). \tag{51}$$

The only difference found between the Cartesian (48) and cylindrical coordinate systems (51) is thus the way the average temperature is determined. In addition, no direct geometry factor appears due to the averaging procedure introduced in (49), and the geometry dependence of the interpolation is implicitly contained in $\overline{T}$. While for Cartesian coordinate systems a logarithmic mean of the temperature is obtained, no explicit expression can be given for $\overline{T}$ in other coordinate systems. However, as will be shown in Section V-A, the influence of the geometry-dependent interpolation is of the order $O(h^2)$, and it is thus justifiable to use the logarithmic mean for other coordinate systems as well. We, therefore, suggest to use $\mathcal{G}_\xi^{\mathrm{cyl}} = 1$. The degree of approximation introduced by this assumption is discussed in detail in Section V.

V. Discussion

In the following, we will discuss the influence of the geometry-dependent interpolation schemes on the resulting equations. The influence on the numerical properties of the final-equation system will be estimated. We will restrict our analysis to the cylindrical coordinates first, because it is the most relevant non-Cartesian coordinate system and, second, because it is the only coordinate system where the integrals are evaluable. Finally, both schemes (with and without the geometry factors $\mathcal{G}$) have been implemented into our device simulator MINIMOS-NT [14]. Of course, both schemes calculate the box volumes and surfaces using (12). To evaluate our theoretical conclusions, a rotationally symmetric thyristor and a surrounding gate FET are investigated.

A. Numerical Properties

Due to the introduction of the geometry factor $\mathcal{G}$, the resulting system matrix of the Poisson equation as well as the continuity equation are slightly changed. To estimate the influence of the geometry factors on the final result, the new system matrix is written as the sum of the original matrix and an incremental matrix. As the inhomogeneity of the partial differential equations is not influenced by the geometry-dependent interpolation scheme, only the influence on the matrix will be considered.

The system matrix itself consists of the linearized equations resulting from the discretization of the Poisson equation (1), (2) and the transport equations (3), (4) as well as the associated boundary conditions.

For a basic analysis, we assume the simulation domain to be 1-D. We then write

$$\mathbf{A}_{\mathcal{G}} = \mathbf{A} + \Delta\mathbf{A}_{\mathcal{G}} \tag{52}$$

with the original matrix

$$\mathbf{A} = \begin{bmatrix} -1-a_1 & a_1 & 0 & 0 \\ 1 & -1-a_2 & a_2 & 0 \\ 0 & 1 & -1-a_3 & a_3 \\ 0 & 0 & \ddots & \ddots \end{bmatrix}$$

$$a_i = \frac{A_i/d_i}{A_{i+1}/d_{i+1}}. \tag{53}$$

Note that each of the matrix lines is multiplied with a factor so the subdiagonal element becomes unity. Even though it is not mentioned explicitly, the inhomogeneity is also affected by this

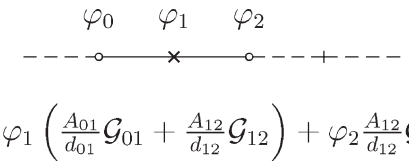

Fig. 4. Discretization scheme for 1-D cylindrical coordinates.

transformation. However, all these calculations are only for error estimation and are not used for assembly. For the assembly, we use, of course, the standard form of the discretization.

As a consequence, the Poisson-system matrix will be tridiagonal and can be easily LU-decomposed. From the LU-decomposition, we can calculate all the eigenvalues of the matrix, and therefore, the spectral norm of the (nongeometry-corrected) system matrix can be easily derived. Without giving a proof, we state that all the eigenvalues are in the interval $[1, a_{\max}+1]$. The deviation of the solution created by a slightly modified matrix can be expressed by the following formula in terms of matrix norms [15]:

$$\frac{\|\Delta\mathbf{x}\|}{\|\mathbf{x}\|} \leq \frac{\mathrm{cond}(\mathbf{A})}{1-\|\mathbf{A}^{-1}\|\,\|\Delta\mathbf{A}_{\mathcal{G}}\|}\frac{\|\Delta\mathbf{A}_{\mathcal{G}}\|}{\|\mathbf{A}\|}. \tag{54}$$

As the matrix increment $\Delta\mathbf{A}_{\mathcal{G}}$, we obtain

$$\Delta\mathbf{A}_{\mathcal{G}} = \begin{bmatrix} \gamma_1 a_1 & -\gamma_1 a_1 & 0 & 0 \\ 0 & \gamma_2 a_2 & -\gamma_2 a_2 & 0 \\ 0 & 0 & \gamma_3 a_3 & -\gamma_3 a_3 \\ 0 & 0 & \ddots & \ddots \end{bmatrix}$$

$$\gamma_i = 1 - \frac{\mathcal{G}_i}{\mathcal{G}_{i+1}}. \tag{55}$$

We use the spectral norm of both $\mathbf{A}$ and $\Delta\mathbf{A}_{\mathcal{G}}$ to evaluate (54) as

$$\frac{\|\Delta\mathbf{x}\|}{\|\mathbf{x}\|} \leq \frac{\max_i \gamma_i a_i}{1-\max_i \gamma_i a_i} \leq \frac{\gamma_{\max} a_{\max}}{1-\gamma_{\max} a_{\max}}. \tag{56}$$

In typical simulations, the maximal geometry-dependent term γ_2 is about $1-10^{-3}$ to $1-10^{-4}$. As a consequence, we obtain typical relative deviations in current and charge of 10^{-3}. From this, we conclude that the geometry factor in the equations can be neglected.

In the following, we will show that the impact of the geometry factor on the solution is smaller than the discretization error. The geometry factors as well as the box distances and surfaces are expressed in terms of h, the radial distance between two mesh points. For the calculation of the factors, we use three points in a radial line with the radii r, $r-h_{12}$, and $r-h_{23}$, see Fig. 4. The box surfaces and distances go with $O(h^2)$ and $O(h)$, respectively. The geometry factors for the interpolation correction between the points is then obtained as

$$\mathcal{G}_{12} = \frac{h_{12}}{(r-h_{12}/2)\ln\left((r-h_{12})/r\right)} \tag{57}$$

$$\mathcal{G}_{23} = \frac{h_{23}}{(r+h_{23}/2)\ln\left((r+h_{23})/r\right)} \tag{58}$$

where it is assumed that h_{12} and h_{23} are either equal (uniform grid) or of the same order of magnitude (quasi-uniform grid).

The deviation matrix $\Delta\mathbf{A}_{\mathcal{G}}$ is determined by γ_2 which reads for uniform grids

$$\gamma_2 = 1 - \frac{\mathcal{G}_{23}}{\mathcal{G}_{12}} = -\frac{h^3}{6r^3} + O(h^4). \tag{59}$$

From the Taylor expansion of (59), we obtain the h dependence of the resulting deviation. After some basic calculations, one finds an $O(h^3)$ dependence for uniform grids and an $O(h^2)$ dependence for quasi-uniform grids. The method of finite volumes, as well as the finite-difference method, lead to numerical errors going with $O(h^2)$ for uniform grids and $O(h)$ for quasi-uniform grids [1]. Thus, if the grid is refined, the numerical error will always be larger than the deviation caused by the geometry factor. Therefore, the use of a properly designed grid seems to be sufficient to keep the influence of the geometry-corrected interpolation smaller than the general discretization error.

B. Singularity Treatment

On some coordinate systems, components of the metric tensor become zero. The regions of the coordinate system in which metric-tensor components vanish are called singular. Only when $\mathcal{G}$ is included, a special treatment of these points is necessary. As we only allow diagonal metric tensors, we just have to consider the direction of the tensor component that vanishes. In the case of cylindrical coordinates, the axis is singular and the direction of singularity is radial ($e_{rr}=0$). Indeed, for symmetry reasons, flux is possible along the axis of rotation but not through it. For the edge between a singular point and a neighboring nonsingular point, homogeneous Neumann boundary conditions can be assumed. For further investigations, we take a look at the associated boxes. Without geometry correction, the calculation is straightforward. For singular points, one solution of the projected Laplace equation $\mathrm{div}\,\mathrm{grad}\, f = 0$ is singular because of flux continuity. Therefore, the total solution can either be constant or singular in the point of singularity.

We neglect singular solutions in our numerical simulations, and therefore, the solution is constant, which means that there is no flux between the singular point and its neighbor.

C. Examples

In the following section, we present two examples: a surrounding gate FET and a thyristor. Both devices are rotationally symmetric and are, therefore, simulated in cylindrical coordinates using our device simulator MINIMOS-NT [14]. The geometry of the investigated FET is shown in Fig. 5. We assume doping levels of 2×10^{20} cm^{-3} in the source and drain regions, an intrinsic channel region, an oxide thickness of 1 nm, and a channel length of 50 nm. The resulting output characteristic for $V_{\mathrm{G}}=1$ V as obtained from both methods is shown in Fig. 6. Also shown is the error introduced when the geometrically corrected interpolation is neglected. As can be clearly seen, the

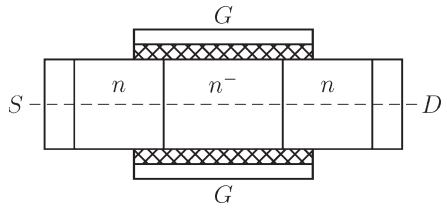

Fig. 5. Surrounding gate FET.

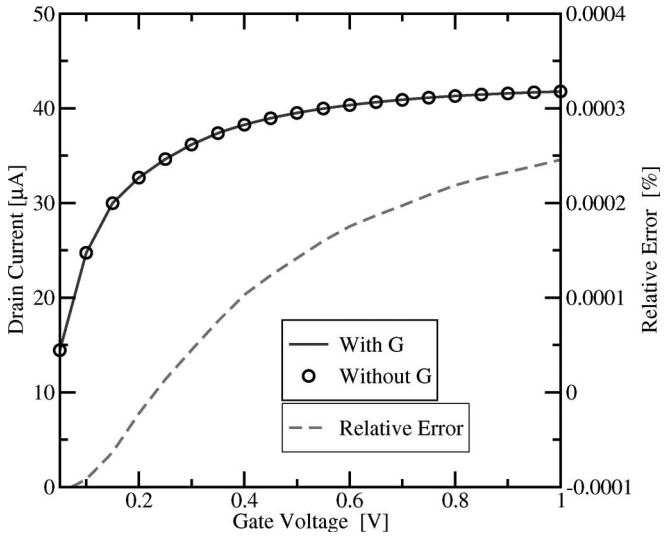

Fig. 6. Surrounding gate FET output characteristics.

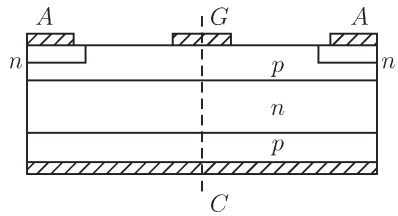

Fig. 7. Rotationally symmetric thyristor.

error is extremely small which confirms the theoretical results given above.

The second example shows a rotationally symmetric thyristor (see Fig. 7) with $n{-}p{-}n{-}p$ doping levels of 10^{19}, 10^{17}, 10^{17}, and 10^{19} cm^{-3}. The device radius is 8 μm and the device thickness is 5 μm. We simulate the ignition of the thyristor by applying a voltage pulse of 0.5 V to the gate with a constant-applied anode voltage of 2 V. As shown in Fig. 8, we obtain a current of 7 A and a typical difference between the geometry corrected and the standard discretization of about 10^{-3}, which further demonstrates the correctness of our initial assumption.

VI. Conclusion

We have proposed discretization schemes for general orthogonal coordinate systems for the Poisson equation and macroscopic-transport equations. Based on the result of the potential interpolation, we obtain a modified-discretization scheme for the isothermal drift-diffusion model. In contrast to the scheme of Matsumoto who used a linear potential interpolation, the use of the solution of the Poisson equation within the same coordinate metric leads to consistent formulas, which are of a similar structure as the standard Scharfetter–Gummel scheme. For the higher order transport equations, we generalized the method of optimum artificial diffusivity and also obtained schemes of the same algebraical structure. In addition to the coordinate-system-dependent calculation of the box volumes and surfaces, these methods introduce a geometry factor, which basically depends on the interpolation scheme of the electrostatic potential in each coordinate system.

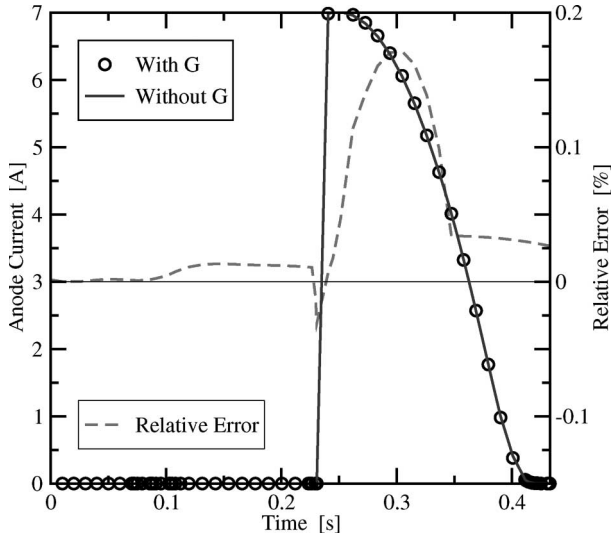

Fig. 8. Thyristor ignition simulated with and without geometry factors.

For the most common non-Cartesian case of rotationally separated cylindrical coordinates, we theoretically investigated the influence of the geometry factor and implemented linear and geometrically adapted discretization schemes for the Poisson equation and the higher order transport equations. This practical evaluation confirms our theoretical results stating that the influence of the geometry factor is small compared to the discretization error of the finite-volume method. In particular, for properly designed grids and meshes, we conclude that these geometry factors can be neglected and, therefore, standard Scharfetter–Gummel schemes together with geometry-adapted box volumes and surfaces are sufficiently accurate for non-Cartesian coordinate systems.

Acknowledgment

The authors would like to thank S. Selberherr as well as P. Schwaha for valuable discussions.

References

[1] S. Selberherr, *Analysis and Simulation of Semiconductor Devices*. New York: Springer-Verlag, 1984.

[2] A. Franz, G. Franz, S. Selberherr, C. Ringhofer, and P. Markowich, "Finite boxes—A generalization of the finite difference method suitable for semiconductor device simulation," *IEEE Trans. Electron Devices*, vol. ED-30, no. 9, pp. 1070–1082, Sep. 1983.

[3] K. Matsumoto, I. Takayanagi, T. Nakamura, and R. Ohta, "The operation mechanism of a charge modulation device (CMD) image sensor," *IEEE Trans. Electron Devices*, vol. 38, no. 5, pp. 989–998, May 1991.

[4] ISE Integrated Systems Engineering AG, *DESSIS-ISE, ISE TCAD Release 9.5*, 2004, Zürich, Switzerland.
[5] Synopsys Corporation, *Medici, Two-Dimensional Device Simulation Program, Version 2002.4*, Feb. 2003, Mountain View, CA.
[6] T. Grasser, T. Tang, H. Kosina, and S. Selberherr, "A review of hydrodynamic and energy-transport models for semiconductor device simulation," *Proc. IEEE*, vol. 91, no. 2, pp. 251–274, Feb. 2003.
[7] T. Grasser, R. Kosik, C. Jungemann, H. Kosina, and S. Selberherr, "Nonparabolic macroscopic transport models for device simulation based on Bulk Monte Carlo Data," *J. Appl. Phys.*, vol. 97, no. 9, pp. 1–12, 2005.
[8] R. Stratton, "Diffusion of hot and cold electrons in semiconductor barriers," *Phys. Rev.*, vol. 126, no. 6, pp. 2002–2014, 1962.
[9] K. Bløtekjær, "Transport equations for electrons in two-valley semiconductors," *IEEE Trans. Electron Devices*, vol. ED-17, no. 1, pp. 38–47, Jan. 1970.
[10] P. J. Frey and P. L. George, *Mesh Generation Application to Finite Elements*. Oxford, U.K.: Hermes, 2000.
[11] W. Neutsch, *Koordinaten*. Heidelberg, Germany: Spektrum Akademischer Verlag, 1995.
[12] A. Forghieri, R. Guerrieri, P. Ciampolini, A. Gnudi, M. Rudan, and G. Baccarani, "A new discretization strategy of the semiconductor equations comprising momentum and energy balance," *IEEE Trans. Comput.-Aided Design Integr. Circuits Syst.*, vol. 7, no. 2, pp. 231–242, Feb. 1988.
[13] T. Tang and M.-K. Ieong, "Discretization of flux densities in device simulations using optimum artificial diffusivity," *IEEE Trans. Comput.-Aided Design Integr. Circuits Syst.*, vol. 14, no. 11, pp. 1309–1315, Nov. 1995.
[14] IμE, *MINIMOS-NT 2.1 User's Guide*, 2004, Wien, Austria: Institut für Mikroelektronik, Technische Universität Wien. [Online]. Available: http://www.iue.tuwien.ac.at/software/minimos-nt
[15] H. R. Schwarz, *Numerische Mathematik*. Stuttgart, Germany: B.G. Teubner Verlag, 1993.

Michael Spevak was born in Vienna, Austria, in 1982. He received the Diplomingenieur degree in electrical engineering from the Technische Universitt Wien, Vienna, in 2004. Since December 2004, he has been working toward the Ph.D. degree at the Institute for Microelectronics, TU Vienna, Austria.

Tibor Grasser (M'05–SM'05) was born in Vienna, Austria, in 1970. He received the Diplomingenieur degree in communications engineering, the Ph.D. degree in technical sciences, and the Venia Docendi in microelectronics from the Technische Universitt Wien, Vienna, in 1995, 1999, and 2002, respectively.

Since 1997, he has headed the Minimos-NT development group, working on the successor of the highly successful MiniMOS program. He was a Visiting Research Engineer for Hitachi Ltd., Tokyo, Japan, and for the Alpha Development Group, Compaq Computer Corporation, Shrewsbury, MA. In 2003, he was appointed Head of the Christian Doppler Laboratory for TCAD in Microelectronics, an industry-funded research group embedded in the Institute for Microelectronics. He is currently employed as an Associate Professor with the Institute for Microelectronics, TU Vienna, Vienna, Austria. His current scientific interests include circuit and device simulation and device modeling.